Journal of Power Sources 210 (2012) 198–203

Contents lists available at SciVerse ScienceDirect

Journal of Power Sources

journal homepage: www.elsevier.com/locate/jpowsour

Analysis of the kinetics of borohydride oxidation in Cu anode for direct borohydride fuel cell

Donghong Duan*, Shibin Liu, Yanping Sun*

College of Chemistry and Chemical Engineering, Taiyuan University of Technology, Taiyuan 030024, China

ARTICLE INFO

Article history:
Received 10 January 2012
Received in revised form 11 March 2012
Accepted 12 March 2012
Available online 22 March 2012

Keywords:
Direct borohydride fuel cell
Cu anode
Borohydride oxidation
Mathematic model

ABSTRACT

A multi-step mechanism is discussed for the oxidation of BH_4^- on Cu anode in NaOH solution. Polarization experiments are conducted in 2 M sodium hydroxide solutions with 0.5, 1.0, and 2.0 M $NaBH_4$ at 25, 50, and 75 °C, respectively. The rate-determining step is the electrochemical oxidation of $BH_{4,ad}^-$ that reacted with OH_{ad}^- at low overpotentials and changes to the competitive adsorption of BH_4^- or OH^- at higher overpotentials. The theoretical predictions are satisfactorily in accordance with the polarization data. However, these predictions deviate from the data at the highest temperature or concentration of BH_4^- because of the bubbling of the side product, H_2.

1. Introduction

Alkali metal borohydride (MBH_4, M = Li, Na, K) is a complex hydride of an anionic compound that contains protide (H^-), with the hydrogen located at the corners of a methane-like tetrahedron, and the metal in the center. MBH_4 has been widely used as a reducing agent, and is considered as an ideal hydrogen storage material because of its high hydrogen content of 10.6 wt.% for $NaBH_4$. In addition, MBH_4 can be used to prepare high-purity H_2 for the PEMFC [1,2] because it does not contain a C element. Hydrogen is released through the following hydrolysis reaction:

$$BH_4^- + 2H_2O \rightarrow BO_2^- + 4H_2 \quad (1)$$

In this hydrolysis process, H^- turns into unstable protium (H^{0*}), which can then be delivered as H_2 gas.

MBH_4 can also be used as an anodic fuel for direct borohydride fuel cell (DBFC) [3,4]. The theoretical oxidation reaction of BH_4^- is

$$BH_4^- + 8OH^- = BO_2^- + 6H_2O + 8e^- \quad (2)$$

In Eq. (2), H^- loses two electrons of the 1s valence electron and is then converted into proton (H^+) contained in H_2O as a reaction product. The process of releasing eight electrons involved in Eq. (2) cannot be completed through a single step. Hence, this reaction is barely found to occur in practice because the anodic reactions on electrodes have to compete with the hydrolysis reaction [5–9]. Therefore, the electrode reaction mechanism is very complicated to draw a conclusion.

Scholars have exerted great efforts to investigate the anodic oxidation mechanism of BH_4^- [10–22]. As early as 1981, Meerakker [18] has conducted further research on the mechanism of $NaBH_4$ anodic oxidation and has summarized a uniform multi-step mechanism. The formation of atomic hydrogen with the dehydrogenation of BH_4^- is considered the first step in the mechanism, followed by the oxidation of BH_4^-. Based on the study of Meerakker, Martins et al. [14] performed a systematic study on Pt electrodes using cyclic voltammetry. This study made a comprehensive summary on the stepwise oxidation mechanism. In Pt, the oxidation of BH_4^- is proposed to follow a CE mechanism sequence. That is, Pt first catalyzes the BH_4^- heterogeneous hydrolysis into stable BH_3OH^-, and the H^- from the intermediate (BH_3OH^-) undergoes further partial oxidation and turns into a single atom H^{0*} by successively losing electrons. Chatenet et al. [15] reported that the multi-step mechanism starts with the adsorption of BH_4^- on the electrode surface, followed by an electro-oxidation reaction. On the other hand, Mirkin et al. [13] proposed that the oxidation of BH_4^- on Au has two reversible processes. Au is a "non-catalytic" electrode, in which the oxidation mechanism is very different from the hydrolysis reaction on Pt. The first stage in the BH_4^- oxidation is considered the formation of monoborane (BH_3) through an ECE reaction mechanism by exchanging two electrons without BH_3OH^-.

In the past few years, fundamental electrochemical studies of BH_4^- were conducted on Au [5,6,12,13,15,17,20–22], Pt [5,6,10,12,14,18,21], Ag [12,15], Pd [6,7,12], Ni [6,8,12,20,21], Zn [23], Cu [6,12,20], hydrogen storage alloys [9], and numerous alloys, such as Pt–Ag [24] and Ni–Pt [25]. These studies used

* Corresponding authors. Tel.: +86 351 6018554; fax: +86 351 6018554.
E-mail addresses: dhduan@163.com (D. Duan), ypsun@tyut.edu.cn (Y. Sun).

0378-7753/$ – see front matter © 2012 Elsevier B.V. All rights reserved.
doi:10.1016/j.jpowsour.2012.03.032

different catalyst morphologies and experimental techniques, including voltammetry at static and rotating electrodes, electrochemical impedance spectroscopy, chronopotentiometry, on-line electrochemical mass spectrometry, surface FTIR [26,27], and electrochemical quartz crystal microbalance [28]. Regardless of the material used as electrode, the four H^- in BH_4^- will still be converted to H^{0*} by successively losing electrons. Moreover, unstable H^{0*} produced as an intermediate may be delivered through the recombination of 2H or further oxidation to emit electrons in a certain electrode potential. Thus, the anodic oxidation reactions of BH_4^- are clearly involved in a novel and complex reaction system of three chemical states of hydrogen valence transformation, namely, H^-, H^{0*}, and H^+ [29].

At present, the mechanism of borohydride oxidation in DBFC is not yet fully understood and is difficult to study experimentally. A mathematical model is imperative in understanding the complex kinetics because the kinetic modeling of the elementary reactions of borohydride oxidation can help determine limiting steps and reactive intermediates to guide the rational design of improved catalysts. However, previous models of the DMFC have been few. To the best of our knowledge, the kinetic models for DBFCs via the kinetic mechanisms of borohydride and oxygen have only been reported in three studies [30–32].

The present study investigates the electrochemical oxidation behavior of BH_4^- on low-cost Cu metal in alkaline solutions and considers that two consecutive elementary steps, namely, electrochemical and prepositive non-electrochemical [13–15], should be concluded in the anodic oxidation mechanism. The latter elementary reaction is hypothesized to occur before the electrochemical steps [13,14]. The different descriptions of the electrochemical reaction mechanism on different electrode materials are combined, and the complex oxidation process of BH_4^- on copper electrode is simplified as follows: BH_4^- and OH^- are adsorbed on the electrode surface first, followed by the electrochemical oxidation reaction. The proposed simple multi-step reaction mechanism can be expressed through the following steps:

$$BH_4^- \underset{k'_1}{\overset{k_1}{\rightleftharpoons}} BH_{4,ad}^- \quad (3)$$

$$OH^- \underset{k'_2}{\overset{k_2}{\rightleftharpoons}} OH_{ad}^- \quad (4)$$

$$BH_{4,ad}^- + 2OH_{ad}^- \xrightarrow{k_3} BO_2^- + 6H^{0*} + 2e^- \quad (5)$$

$$H^{0*} + OH_{ad}^- \xrightarrow{k_4} H_2O + e^- \quad (6)$$

$$H^{0*} + H^{0*} \xrightarrow{k_5} H_2 \quad (7)$$

where k is the reaction rate constant. In this process, BH_4^- and OH^- in the electrolyte are first adsorbed on the Cu surface to generate the adsorbed $BH_{4,ad}^-$ and OH_{ad}^-. When contact is made with the OH_{ad}^-, BH_4^- will give an electron from the 1s valence electron to H^+ as an electron-donating species because of the relatively loose electron cloud density of H^- bound to the nucleus. The redox reaction generates BO_2^- and a highly reactive radical hydrogen (H^{0*}), simultaneously releasing two electrons. Unstable H^{0*} then undergoes two kinds of reaction pathways on the electrode surface. One is the recombination of 2 H^{0*} into gas, and the other is the combination of H^{0*} with OH_{ad}^- and its conversion into a naked proton H^+ by releasing electrons. The whole electrode reaction refers to three hydrogen valence state transformations, namely H^-, H^{0*}, and H^+. Moreover, the electronic number that is apparently released depends on the competition between Eqs. (6) and (7).

Based on the proposed reaction mechanism, the kinetic equation in the present study involved both coverage ratios θ_B and θ_{OH} of $BH_{4,ad}^-$ and OH_{ad}^- adsorbed on the surface of Cu anode deduced by the steady state approximation theory. To understand the operation behavior and provide preliminary theory basis on the reaction engineering of DBFC, kinetic parameters are obtained, and theoretical polarization curves are calculated. Lastly, electrode dynamic rules are analyzed quantitatively according to experimental polarization data at different temperatures and $NaBH_4$ concentrations of Cu.

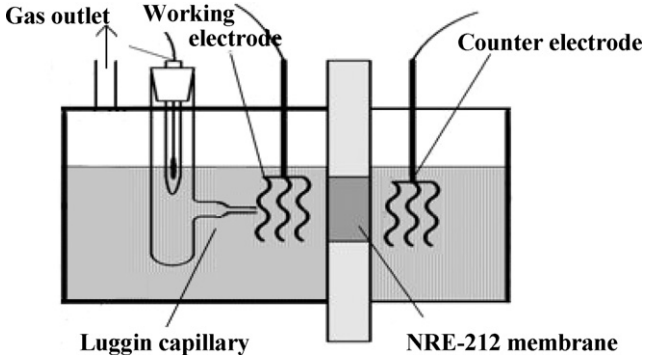

Fig. 1. Schematic diagram of the experiment setup.

2. Experimental

2.1. Reagents and materials

The materials and chemicals used during the tests are listed as follows: $NaBH_4$ (98%, Ke-long, Chengdu), NaOH (98%, Ke Miou, Tianjin), H_2O_2 (30%, Tianjin) and HCl (Taiyuan Chemical Industry), All chemical reagents were of analytical grade and all solutions were prepared with doubly distilled water.

The Cu electrode employed in our experiment was a meshy copper net (99.97%, mesh 100, Hebei-Anping). To eliminate the oxides on the surface of Cu electrode, dipped it in sulphuric acid with the concentration of 1.0 mol L^{-1} for about 30 min, next in acetone with the same way, and then washed with distilled water, dried with filter paper at last.

The NRE-212 membrane (DuPont) was pretreated by heating solutions to 80°C in a 5 wt.% H_2O_2 solutions for 1 h, and then also immersed in 1 M NaOH for another 1 h. At last, the pretreated membrane were washed and stored in deionized water for use.

2.2. Performance testing

Anodic performance of DBFC was evaluated by a homemade electrochemical testing system. The schematic diagram of the experimental set-up is shown in Fig. 1. The Cu electrode with 1 cm × 1 cm was used as working electrode, a Pt net (50 mesh, Tianjin Aida) with 1 cm × 1 cm as the counter electrode and a Hg/Hg_2Cl_2 (Model 232) electrode as the reference electrode. The dimension of the anode compartment and cathode compartment are both 3 cm × 4 cm × 5 cm, and the exposed area of the membrane is 1 cm × 1 cm. The catholyte and anolyte are separated by the pretreated NRE-212 membrane. The anolyte was 2 M NaOH with n M $NaBH_4$ (n = 0.5, 1, 2) and catholyte composed of 2.0 M HCl + 4.5 M H_2O_2. The device was placed in constant temperature water-bath to control the testing temperature. The ultrahigh-purity nitrogen has been supplied to the anolyte for 30 min before each experiment. Polarization curves are measured by a computer-controlled VMPIII multicenter potentiostat (American PAR Inc.) and the EC-Lab software was used to deal with the experimental dates. All potential values in this work were referred vs. the Hg/Hg_2Cl_2 electrode (SCE), and the amount of hydrogen

generated during operation was measured using a flow meter and the volume was converted into the value at the standard temperature and pressure (STP) before hydrogen evolution rates were calculated.

3. Model development

3.1. Assumptions

In the model development, the following assumptions are made to simplify the mathematical treatment:

(1) The system is at a steady state. (2) The system is operated isothermally. (3) The electrode surface concentration is equal to the bulk concentration, that is, it remains unaffected on the transfer process. (4) The electrode-kinetics for BH_4^- oxidation at the Cu anode can be described by the Tafel equation. (5) The adsorption of the components on the electrode surface is in accordance with the Langmuir ideal adsorption. (6) The effect of the two-phase flow formed by the generated hydrogen in the transfer process is ignored.

3.2. Analytical solution

When the reaction system reaches a steady state, the rate of the reaction steps of Eqs. (3)–(5) should be equal (i.e., $r_1 = r_2 = r_3$), and only one is needed to represent the total reaction rate of the series. In the present paper, the expression of r_3 for the surface electrochemical reaction step [Eq. (5)] involving information on all elementary steps (including BH_4^- and OH^- adsorption) was selected as the total reaction rate expression.

The rate expression of Eq. (5) is given as follows:

$$r_3 = k_3\theta_B\theta_{OH}^2 e^{((\alpha F\eta)/(RT))} \tag{8}$$

The rate of changes in the surface coverage of different intermediate species with respect to time can be derived as follows:

$$\frac{d\theta_B}{dt} = k_1 C_B(1-\theta_B-\theta_{OH}) - k'_1\theta_B - k_3\theta_B\theta_{OH}^2 e^{((\alpha F\eta)/(RT))} \tag{9}$$

$$\frac{d\theta_{OH}}{dt} = k_2 C_{OH}(1-\theta_B-\theta_{OH}) - k'_2\theta_{OH} - k_3\theta_B\theta_{OH}^2 e^{((\alpha F\eta)/(RT))} - k_5 C_H\theta_{OH} e^{((\alpha F\eta)/(RT))} \tag{10}$$

In the present study, to reduce the number of kinetic parameters, the high-activity H^{0*} generated in Eq. (5) is assumed to be immediately consumed by Eq. (6) or (7), making the concentration of H^{0*} in the solution very low. As considered in the literature [15], the activation adsorption of BH_4^- [Eq. (3)] is an irreversible reaction; hence, $k_1 > k_1^1$.

At the steady state, the surface coverage of adsorbed species does not change with time. Thus, when $C_H \approx 0$ and $k'_1 \approx 0$, the steady state solution of Eqs. (9) and (10) can be given as follows:

$$\theta_B = \frac{k_1 C_B(1-\theta_{OH})}{k_1 C_B + k_3\theta_{OH}^2 e^{\beta}} \tag{11}$$

$$\theta_B = \frac{k_2 C_{OH}(1-\theta_{OH}) - k'_2\theta_{OH}}{k_2 C_{OH} + k_3\theta_{OH}^2 e^{\beta}} \tag{12}$$

where $\beta = ((\alpha F\eta)/(RT))$. The above simultaneous equations can be solved to give the surface coverage of θ_B and θ_{OH}, and then substituted in the overall reaction rate in Eq. (8). Using the Faraday's law, the corresponding anode current density (J) can be obtained from Eq. (13):

$$J = nFr_3 = nFk_3\theta_B\theta_{OH}^2 e^{\beta} \tag{13}$$

Table 1
Kinetic parameters used in the model for cell.

Kinetic parameters	25 °C	50 °C	75 °C
k_1 [m s^{-1}]	2.6×10^{-6}	5.3×10^{-6}	7.6×10^{-6}
k'_2 [mol m^{-2} s^{-1}]	1.0×10^{-6}	1.0×10^{-6}	1.0×10^{-6}
k_3 [mol m^{-2} s^{-1}]	1.7×10^{-7}	3.6×10^{-7}	8.2×10^{-7}
α	0.39	0.40	0.49

4. Results and discussion

Table 1 shows the constants and kinetic parameters used in the model. One set of kinetic parameters, corresponding to the elementary reaction steps, is regressed, which fit with the experimental polarization data for bulk sodium borohydride with concentrations 0.5, 1.0 and 2.0 M at 25, 50, and 75 °C, respectively. The value of α in the case of borohydride oxidation is 0.39. Verma [30] and Ayse Elif Sanli [31] used an α value of 0.3. The rate constants k_1, k'_2, and k_3 for electrooxidation and the adsorption and desorption constants for $NaBH_4$ on electrode surface are not reported in the literature. However, they are of the same order of magnitude to those found in the literature for similar reactions involving methanol [33,34]. According to the kinetic parameters, theoretical polarization curves and coverage ratio based on the Langmuir ideal adsorption are calculated and compared with the experimental data. Theoretical analysis of the experiment results is then conducted.

4.1. Coverage of intermediate species on the electrode surface

The intrinsic reaction rate or current density is proportional to both fractional coverage θ_B and θ_{OH} of $BH_{4,ad}^-$ and OH_{ad}^- adsorbed on the surface of the Cu anode, which are functions of BH_4^- and OH^- concentrations, temperature, and overpotential. The variations of fractional coverage with overpotentials η can be obtained by solving the nonlinear Eqs. (11) and (12).

4.1.1. Effect of temperature on the surface coverage

The surface coverage of $BH_{4,ad}^-$ and OH_{ad}^- at different temperatures and 1.0 M sodium borohydride solution is depicted in Fig. 2. As shown in Fig. 2, the changes in the surface coverage are similar at 25, 50, and 75 °C. Initially, θ_B and θ_{OH} do not change with the increase in the wide potential range between 0 and 0.50 V. This result can be attributed to the slow rate of the surface electrochemical reaction step [Eq. (5)], and the adsorption equilibrium approximately achieved by the chemical adsorption [Eqs. (3) and (4)]. The surface

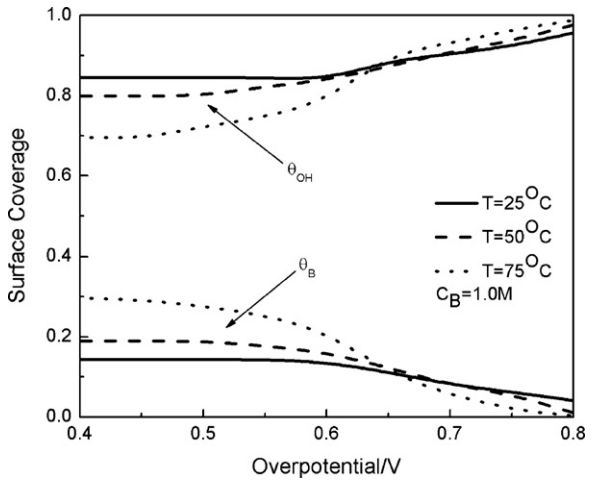

Fig. 2. Surface coverage (θ_B and θ_{OH}) with varying overpotential at different operating temperature.

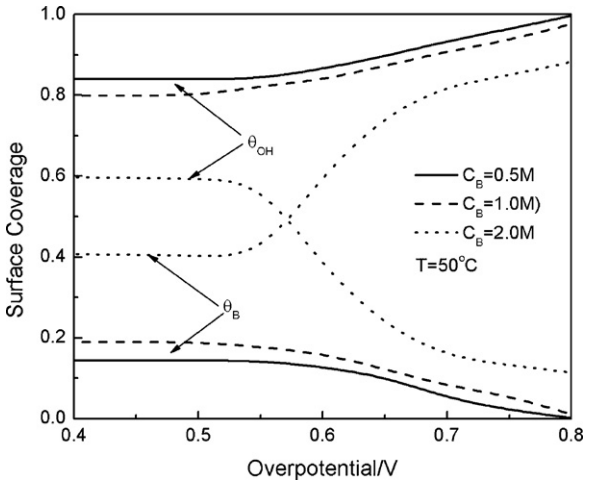

Fig. 3. Surface coverage (θ_B and θ_{OH}) with varying overpotential at different sodium borohydride concentration at 50 °C.

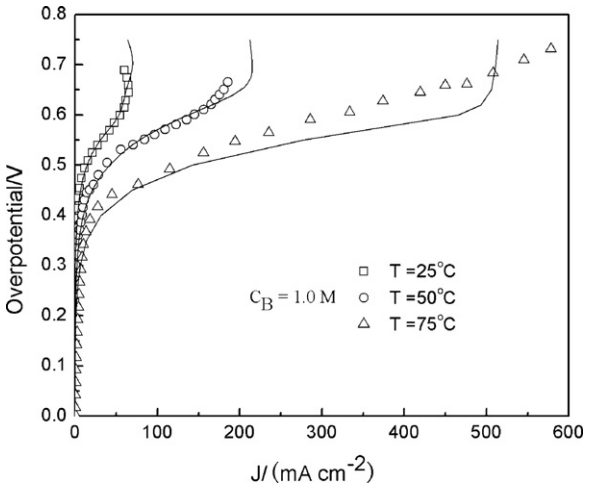

Fig. 4. Polarization curves of model (line) vs. experimental fit at 25 °C, 50 °C and 75 °C with 1.0 M $NaBH_4$ concentrations.

coverage of $BH^-_{4,ad}$ and θ_B gradually decreases to near 0 at η above 0.5 V, whereas θ_{OH} gradually increases to near 1 for potentials above 0.5 V. This result can be attributed to the accelerated rate of surface electrochemical reaction [Eq. (3)] with increasing anode potential, which resulted in the rapid reduction of θ_B in the electrode surface, and the occupation of the adsorption sites by θ_{OH}.

Therefore, the electrochemical reaction [Eq. (3)] may be the rate-limiting step at low η. Therefore, no rate-limiting step exists in the transition region of the intermediate values of η. In effect, the rate-limiting step with high η is the adsorption rate of BH_4^- on the surfaces of the electrodes.

In addition, temperature has opposite effects on the surface coverage of BH_4^- and OH^- on the catalyst site. An increase in temperature decreases θ_{OH} and increases θ_B.

4.1.2. Effect of bulk concentration on the surface coverage

The surface coverage of $BH^-_{4,ad}$ and OH^-_{ad} at different sodium borohydride concentrations at 50 °C is shown in Fig. 3. As shown in Fig. 3, the surface coverage curves for both 0.5 and 1.0 M $NaBH_4$ possess the same trend. However, the surface coverage curves for 2.0 M $NaBH_4$ are obviously different from those in 0.5 and 1.0 M $NaBH_4$ concentrations. The surface coverage of $BH^-_{4,ad}$ and θ_B obviously increases, whereas that of θ_{OH} sharply decreases for potentials above 0.5 V in 2.0 M $NaBH_4$ concentration. This phenomenon is in favor of the chemical adsorption in 2.0 M $NaBH_4$ concentration, resulting in a significant increase in θ_B and a corresponding decrease in θ_{OH} in the electrode surface. With increasing potential, the electrode surface reaction rate is accelerated, and the consumption of θ_{OH} on the adsorption sites is occupied by $BH^-_{4,ad}$.

Therefore, the rate-limiting step in 2.0 M sodium borohydride concentration is initially the surface electrochemical reaction [Eq. (5)], but will later turn into a hydroxyl chemical adsorption reaction [Eq. (4)]. This finding can be attributed to the competitive adsorption between $BH^-_{4,ad}$ and OH^-_{ad} on the electrode surface. The surface coverage is either increasing or decreasing with the changes in the reaction conditions. This value is maximum in Eq. (8), which corresponds to the optimal BH_4^- concentration.

4.2. Model validation

The polarization curve of an electrode describes the variation in the applied surface overpotential and current density. The surface coverage of θ_B and θ_{OH} is obtained by solving Eqs. (11) and (12). The calculated value is then substituted to Eq. (13) to obtain the final model value. Figs. 4 and 5 show the fit of the model to the experimental data at different $NaBH_4$ concentrations and temperatures from the Cu anode described in the previous section. As shown in Figs. 4 and 5, the model is in quite a good agreement with the BH_4^- oxidation kinetics at low currents at 25 and 50 °C. However, a slight departure is observed from the data at high currents at 70 °C.

Fig. 4 shows the experimental and modeling results of polarization behavior for 1.0 M sodium borohydride solutions at 25, 50, and 75 °C, and the polarization curve response of BH_4^- oxidation behavior for a small-scale single DBFC cell. The experimental polarization curve showed three regions: the region at low η (approximately below 0.4 V), the region at high η (approximately above 0.6 V), and the transitional region at medium η. One characteristic that is observed is the large initial drop in potential at low current densities in all concentrations at low η. These results show that anode polarization does not vary with BH_4^- concentration, and that the apparent reaction order is nearly zero with respect to BH_4^- concentration. The rate-determining step is the electrode oxidation reaction of $BH^-_{4,ad}$ at this region. The anode polarization exhibits a characteristic at medium η, in which the current density J increases rapidly with increasing η. Moreover, at high η (approximately above 0.6 V), J eventually approaches a maximum current density that does not vary with η. In addition, this

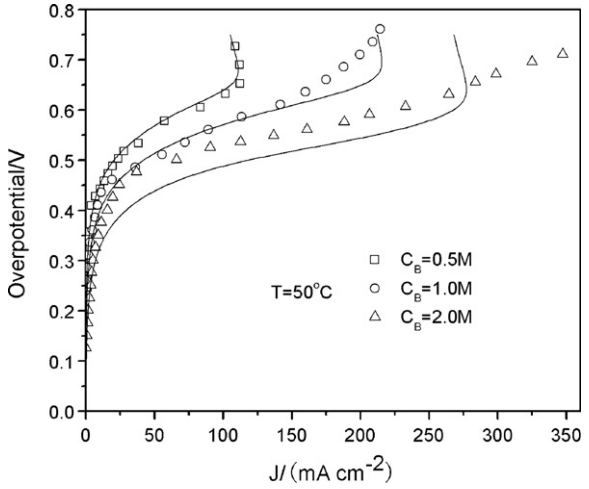

Fig. 5. Polarization curves of model (line) vs. experimental fit at 50 °C with varying $NaBH_4$ concentrations.

maximum current density is an "adsorption limiting current density" J_C, which is almost proportional to the bulk concentration of BH_4^- and caused by the limiting elemental step rather than the familiar "limiting current density" caused by the external mass transport. Lastly, the electrode reaction is controlled by chemical steps, such as the adsorption of $BH_{4,ad}^-$ and OH_{ad}^- on the electrode surface with a controlling current density J_C.

As shown in Fig. 4, the effect of temperature on the current density is important. As expected, increasing temperature increases current density. The current density at η above 0.65 V is 65,214,503 mA cm^{-2}, which increased by 3.3 and 2.4 times to the prior temperature. The activation energies determined from the Arrhenius plots of the rate constants (Table 1) and inverse temperature (not shown) of the surface reaction [Eq. (5)] and $BH_{4,ad}^-$ adsorption reactions [Eq. (4)] were 39.28 and 37.2 kJ mol^{-1}, respectively. An increase in temperature increases the oxidation reaction rate of electrode surface and adsorption control current density J_C of BH_4^-. By contrast, the data at high currents exhibit a linear trend at 75 °C. This result may be attributed to the important effect of mass transport on the exterior surface of the anode at high currents because H_2 bubbles may block the diffusion of BH_4^-.

The fit of model to the experimental data from a cell operating at 25, 50, and 75 °C with varying sodium borohydride concentrations (i.e., 0.5, 1, and 2 M, respectively) is shown in Fig. 5. All the polarization curves exhibit the same trend. At low current densities, the anode polarization does not vary with BH_4^- concentration, and the apparent reaction order is nearly zero with respect to BH_4^-. At high η, limiting current densities are approached because of the effect of adsorption in the anode. This maximum current density is 110,214,398 mA cm^{-2} at 50 °C for the different BH_4^- concentrations. This value is almost proportional to the bulk concentration of BH_4^-. This phenomenon indicates that the apparent reaction order is 1 with respect to BH_4^-. Therefore, the apparent reaction order with respect to BH_4^- changes from 0 to 1 at medium η.

As shown in Figs. 4 and 5, the predicted values agree well with experimental data at low and medium η. However, considerable departure from the data that show a linear trend was found at high polarization conditions (high temperatures, high BH_4^- concentrations, and high η). The experimental current densities with 1.0 M BH_4^- at 75 °C and 2.0 M BH_4^- at 50 °C are lower compared with those predicted. This result can be attributed to the important effect of mass transport on the exterior surface of the anode at high currents because H_2 bubbles may block the transfer of BH_4^- from the bulk into the surface of the anode [35]. The model developed in the present study does not take into account the effect of two-phase flows caused by H_2. This departure of experimental data from the predicted data may be accounted to the hydrogen gas generation from sodium borohydride at high temperature and high BH_4^- concentrations.

Overall, two typical elementary reactions steps can be concluded. One is the electrochemical reaction that liberates electron and becomes the rate-limiting step at low η. The low η region can be called the electrochemical control region. The other step is the non-electrochemical process that occurs prior to the electrochemical steps. With increasing η, the maximum current density, which is independent of η, approaches at high η. The processes are then controlled by nonelectrochemical steps. This maximum current density is an "adsorption limiting current density", J_C, rather than the familiar "limiting current density" caused by external mass transport.

Some of the polarization curves in Figs. 4 and 5 exhibit a significant curving back phenomenon. This phenomenon can be attributed to the competition between electrochemical and nonelectrochemical reactions in two parallel reaction routes depending on the electrode potential (e.g., the adsorption of BH_4^- and OH^- as well as the additional intermediates). These details affecting the kinetic reaction mechanism require in-depth study in the future.

5. Conclusion

The present study developed a proposed kinetic model based on a multi-step mechanism for BH_4^- oxidation on Cu anode in NaOH solution. The models can predict the performance of the electrode and the behavior of surface coverage of intermediates as a function of cell temperature, anode η, and BH_4^- concentration.

The theoretical analysis and the experiment results suggest that the electrochemical oxidation reaction step is the rate-determining step at low η. With the increase in the anode potential, the competitive adsorption of intermediates gradually becomes the rate-determining step at high η.

The models are validated using the experimental data at different BH_4^- concentrations and temperatures for the Cu anode. The model did not take into account the two-phase flow, which may explain the departure of the experimental data from the predicted polarization curves at high concentration and high apparent current densities.

The present study can also serve as a basis for future studies on the theoretical performance of the anodes in DBFC and other direct liquid-feed fuel cells [36].

Acknowledgements

This work was supported by a grant from the National Natural Science Foundation of China (20776091) and the Ph.D. Programs Foundation of Ministry of Education of China (200801120010).

References

[1] S.C. Amendola, S.L. Sharp-Goldman, M.S. Janjua, M.T. Kelly, P.J. Petillo, M. Binder, J. Power Sources 85 (2000) 186–189.
[2] P. Krishnan, T.H. Yang, W.Y. Lee, C.S. Kim, J. Power Sources 143 (2005) 17–23.
[3] D.A. Finkelstein, D.J. Jones, K. Hernandez-Burgos, H.D. Abruña, J. Power Sources 196 (2011) 6223–6227.
[4] M.H. Atwana, D.O. Northwooda, E.L. Gyengeb, Int. J. Hydrogen Energy 32 (2007) 3116–3125.
[5] E. Gyenge, Electrochim. Acta 49 (2004) 965–978.
[6] B.H. Liu, Z.P. Li, S. Suda, Electrochim. Acta 49 (2004) 3097–3105.
[7] C. Celik, F.G.B. San, H.I. Sarac, Int. J. Hydrogen Energy 35 (2010) 8678–8682.
[8] B.H. Liu, Z.P. Li, S. Suda, J. Electrochem. Soc. 150 (2003) A398–A402.
[9] S.M. Lee, J.H. Kim, H.H. Lee, P.S. Lee, J.Y. Lee, J. Electrochem. Soc. 149 (2002) A603–A606.
[10] J.P. Elder, A. Hickling, Trans. Faraday Soc. 58 (1962) 1852–1864.
[11] M.E. Indig, R.N. Snyder, J. Electrochem. Soc. 109 (1962) 1104–1106.
[12] O. Izumi, W. Osamu, H. Shiro, J. Electrochem. Soc. 132 (1985) 2323–2330.
[13] M.V. Mirkin, H. Yang, A.J. Bard, J. Electrochem. Soc. 139 (1992) 2212–2217.
[14] J.I. Martins, M.C. Nunes, R. Koch, L. Martins, M. Bazzaoui, Electrochim. Acta 52 (2007) 6443–6449.
[15] M. Chatenet, F. Micound, I. Roche, E. Chainet, Electrochim. Acta 51 (2006) 5459–5467.
[16] J.H. Morris, H.J. Gysling, D. Reed, Chem. Rev. 85 (1985) 51–76.
[17] P.I. Iotova, S.V. Kalcheva, A.M. Bond, Electrochim. Acta 54 (2009) 7236–7241.
[18] J.E.A.M. Meerakker, J. Appl. Electrochem. 11 (1981), 387–393, 395–400.
[19] M.C.S. Escano, E. Gyenge, R.L. Arevalo, H. Kasai, J. Phys. Chem. C 115 (2011) 19883–19889.
[20] K.L. Wang, J.T. Lu, L. Zhuang, Catal. Today 170 (2011) 99–109.
[21] H. Dong, R.X. Feng, X.P. Ai, Y.L. Cao, H.X. Yang, C.S. Cha, J. Phys. Chem. B 109 (2005) 10896–10901.
[22] D.M.F. Santos, C.A.C. Sequeira, Electrochim. Acta 55 (2010) 6775–6781.
[23] D.M.F. Santos, C.A.C. Sequeira, J. Electrochem. Soc. 157 (2010) B13–B19.
[24] B.M. Concha, M. Chatenet, Electrochim. Acta 54 (2009) 6119–6129.
[25] X. Geng, H. Zhang, W. Ye, Y. Ma, H. Zhong, J. Power Sources 185 (2008) 627–632.
[26] B.M. Concha, M. Chatenet, C. Coutanceau, F. Hahn, Electrochem. Commun. 11 (2009) 223–226.
[27] B.M. Concha, M. Chatenet, E.A. Ticianelli, F.H.B. Lima, J. Phys. Chem. C 115 (2011) 12439–12447.
[28] V.W.S. Lam, D.C.W. Kannangara, A. Alfantazi, E.L. Gyenge, J. Phys. Chem. C 115 (2011) 2727–2737.

[29] Z.P. Li, B.H. Liu, K. Arai, N. Morigazaki, S. Suda, J. Alloys Compd. 356–357 (2003) 469–474.
[30] A. Verma, S. Basu, J. Power Sources 168 (2007) 200–210.
[31] A.E. Sanli, M.L. Aksu, B.Z. Uysal, Int. J. Hydrogen Energy 36 (2011) 8542–8549.
[32] G. Rostamikia, A.J. Mendoza, M.A. Hickner, M.J. Janik, J. Power Sources 196 (2011) 9228–9237.
[33] M.R. Shivhare, C.L. Jackson, K. Scott, E.B. Martin, J. Power Sources 173 (2007) 240–248.
[34] M.R. Shivhare, R.G. Allen, K. Scott, A.J. Morris, E.B. Martin, J. Electroanal. Chem. 595 (2006) 145–151.
[35] Z.P. Li, B.H. Liu, J.K. Zhu, S. Suda, J. Power Sources 163 (2006) 555–559.
[36] Y.P. Sun, L. Xing, K. Scott, J. Power Sources 195 (2010) 1–10.